

Comparative study between sliding mode control and the vector control of a brushless doubly fed reluctance generator based on wind energy conversion systems

Introduction. Nowadays, global investment in renewable energy sources has been growing intensely. In particular, we mention here that wind source of energy has grown recently. **Purpose.** Comparative study between sliding mode control and vector control of a brushless doubly fed reluctance generator based on wind energy conversion systems. **Methods.** This paper deals with conceptual analysis and comparative study of two control techniques of a promising low-cost brushless doubly-fed reluctance generator for variable-speed wind turbine considering maximum power point tracking. This machine's growing interest because of the partially rated power electronics and the high reliability of the brushless design while offering performance competitive to its famous spring counterpart, the doubly-fed induction generator. We are particularly interested in comparing two kinds of control methods. We indicate here the direct vector control based on Proportional-Integral controller and sliding mode controller. **Results.** Simulation results show the optimized performances of the vector control strategy based on a sliding mode controller. We observe high performances in terms of response time and reference tracking without overshoots through the response characteristics. The decoupling, the stability, and the convergence towards the equilibrium are assured. References 29, figures 10.

Key words: wind energy, brushless doubly fed reluctance generator, vector control, sliding mode controller, maximum power point tracking.

Вступ. Нині глобальні інвестиції у відновлювані джерела енергії стрімко зростають. Зокрема, звернемо увагу, що останнім часом має місце зростання вітряних джерел енергії. **Мета.** Порівняльне дослідження між управлінням ковзним режимом та векторним управлінням безщіткового реактивного генератора з подвійним живленням на основі систем перетворення енергії вітру. **Методи.** Стаття присвячена концептуальному аналізу та порівняльному дослідженню двох методів управління перспективним недорогим безщітковим реактивним генератором з подвійним живленням для вітряної турбіни зі змінною швидкістю з урахуванням відстеження точки максимальної потужності. Інтерес до цієї машини зростає частково завдяки силовій електроніці, а також високій надійності безщіткової конструкції, яка при цьому пропонує характеристики, порівняні з його загальновідомим пружинним аналогом, індукційним генератором з подвійним живленням. Автори особливо зацікавлені у порівнянні двох видів методів управління. Автори вказують тут на пряме векторне управління на основі пропорційно-інтегрального регулятора та регулятора ковзного режиму. **Результати.** Результати моделювання показують оптимізовані характеристики векторної стратегії управління на основі контролера ковзного режиму. Спостерігаються високі показники з точки зору часу відгуку та відстеження еталонних значень без перевищення показників відгуку. Розв'язка, стабільність та прагнення до рівноваги гарантуються. Бібл. 29, рис. 10.

Ключові слова: енергія вітру, безщітковий реактивний генератор з подвійним живленням, векторне управління, регулятор ковзного режиму, відстеження точки максимальної потужності.

1. Introduction. The earth climate can be seriously influenced by increasing green house gas emissions from conventional energy sources (such as oil and coal) as well as the growing concern of depletion of these resources in the near future [1]. Wind turbine is one way to generate electricity from renewable sources, mainly because it is clean and economically viable [2]. At the same time, there has been a rapid development of related wind turbine [3].

The wind turbine is a very effective component in wind energy conversion systems (WECS) that converts the wind kinetic energy into mechanical energy that can be used to derive an electrical generator. The wind turbine generator converts the output mechanical energy of the wind turbine into electric power [4]. It can be connected either to stand-alone loads or connected to the utility grid [5].

Wind turbine generators used in wind energy conversion systems can be classified into two types: fixed speed wind turbine (FSWT) and variable speed wind turbine (VSWT). For the first one, the generator is connected directly to the grid without any intermediate of power electronic converters (PECs), and for the other one, the generator is connected through PECs [6–8]. Their findings show that the VSWT provides better energy capture over the FSWT because it can quickly adapt to a wide range of wind speed variations [9]. For this reason, the model considered in this research is the VSWT coupled to a Brushless Doubly Fed Reluctance Generator (BDFRG).

The brushless doubly-fed generator (BDFG) is a prominent economical solution to reliability and maintenance problems of brushes and slip-rings with the traditional doubly-fed induction generator (DFIG) in WECS [10, 11]. The BDFRG merits have inspired the research on its design, control, and grid integration aspects targeting WECS as one of the leading applications [12]. The strengths of this design include simple infrastructure, economical, reliable high efficiency, and robust power factor control capability [13]. Due to its high reliability these machines are also adaptable in air craft industry but some of design challenges include harsh aerodynamic and complex rotor design [14]. The background and fundamental structure of the Brushless Doubly Fed Reluctance Motor (BDFRM) was described in [15].

Control research [16], similar in context to that conducted on the BDFG [17], and DFIG [18], has been carried out on the BDFRM(G) involving: scalar control, voltage vector-oriented control (VC) [19], direct torque and flux control (DTC) [20], torque, and reactive power control (TQC) [21, 22], direct power control (DPC) [23], sliding-mode power control [24], and even nonlinear multiple-input-multiple-output control [3]. Recently, sliding mode control (SMC) was integrated largely in the command of nonlinear systems [25].

The variable structure control possesses this robustness using the sliding mode controller. It offers

excellent performances compared to unmodelled dynamics [26], insensitivity to parameter variation, external disturbance rejection, and fast dynamic [27].

The proposed system comprises a wind turbine, a BDFRG, an inverter, and a vector control based on PI controller and sliding mode controller.

This paper is organized as follows. A description of the studied WECS is presented in section 2. In section 3 the modeling of the wind turbine and the control of the maximum power point tracking (MPPT) are provided. Then, the BDFRG is modeled in Section 4. The vector control of BDFRG is given in Section 5. The sliding mode control is described in Section 6. The sliding mode control of the BDFRG is given in Section 7. Finally, simulation results and interpretations are presented in Section 8.

2. Description of the studied WECS. The WECS adopted here is shown in Fig. 1. The proposed system is constituted of a wind turbine, BDFRG, inverter, and power control. The BDFRG has two stator windings of different pole numbers. Generally, different applied frequencies (Fig. 1): the primary (power) winding is grid-connected, and the secondary (control) winding is converter fed. The performance of the proposed system has been tested to prove the MPPT control. The independent control of grid active and reactive powers using stator flux oriented control technique is used to test the ability to operate in two quadrant modes (sub-synchronous and super-synchronous modes).

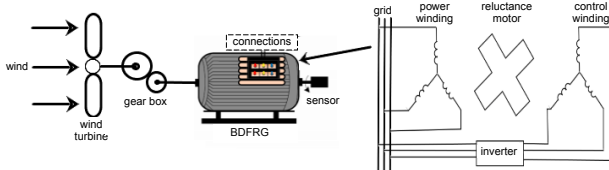


Fig. 1. Conceptual diagram of the BDFRG-based WECS

3. Modeling of the wind turbine. The mechanical power extracted by the turbine from the wind is defined as:

$$P_t = \frac{1}{2} \cdot \rho \cdot A \cdot C_p \cdot V^3, \quad (1)$$

where ρ is the air density; $A = \pi R^2$ is the rotor swept area; R is the turbine radius; C_p is the power coefficient; V is the wind speed.

The power coefficient C_p represents the aerodynamic efficiency of the wind turbine. It depends on the tip speed ratio λ and the pitch angle β (Fig. 2, 3). The tip speed ratio is given as:

$$\lambda = \frac{\Omega_t \cdot R}{V}, \quad (2)$$

where Ω_t is the turbine speed.

For our example, the power coefficient C_p is given by the following equations

$$C_p(\lambda, \beta) = 0.5176 \cdot \left(\frac{116}{\lambda_x} - 0.4 \cdot \beta - 5 \right) \cdot e^{-\frac{21}{\lambda_x}} + 0.0068 \cdot \lambda, \quad (3)$$

where

$$\frac{1}{\lambda_x} = \frac{1}{\lambda + 0.08 \cdot \beta} - \frac{0.035}{\beta^3 + 1}. \quad (4)$$

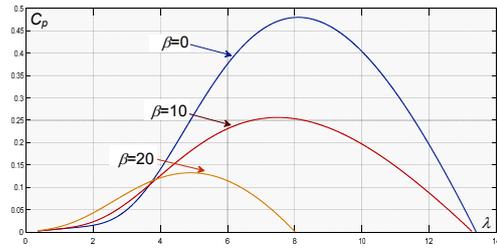


Fig. 2. Characteristics of the wind turbine power coefficient C_p with the tip speed ratio λ at different values of the blade pitch angle β

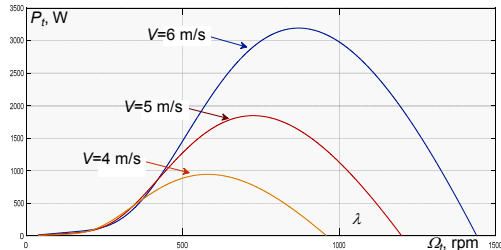


Fig. 3. Power speed characteristics for different wind speeds

The maximum value of C_p ($C_{p \max} = 0.48$) is for $\beta = 0$ degree and for $\lambda = 8.1$. The turbine torque T_t can be written as:

$$T_t = P_t / \Omega_t. \quad (5)$$

The mechanical speed of the generator Ω_m and the torque of the turbine referred to the generator T_m are given by:

$$\begin{cases} \Omega_m = \Omega_t \cdot G; \\ T_m = T_t / G, \end{cases} \quad (6)$$

where G is the gearbox ratio.

The mechanical equation of the system can be characterized by:

$$J \cdot \frac{d\Omega_m}{dt} = T_m - T_e - f \cdot \Omega_m, \quad (7)$$

where J is the equivalent total inertia of the generator shaft; f is the equivalent total friction coefficient; T_e is the electromagnetic torque.

To extract the maximum power from the wind turbine the electromagnetic torque command of the BDFRG T_{e-ref} should be determined at the optimal value of the tip speed ratio and the corresponding maximum value of wind turbine power coefficient.

4. Mathematical model of BDFRG. The electrical equations of the BDFRG in the (d - q) Park reference frame are given by:

$$\begin{cases} U_{pd} = R_p \cdot I_{pd} + \frac{d\Phi_{pd}}{dt} - \omega_p \cdot \psi_{pq}; \\ U_{pq} = R_p \cdot I_{pq} + \frac{d\Phi_{pq}}{dt} + \omega_p \cdot \psi_{pd}; \\ U_{sd} = R_s \cdot I_{sd} + \frac{d\Phi_{sd}}{dt} - (\omega_r - \omega) \cdot \psi_{sq}; \\ U_{sq} = R_s \cdot I_{sq} + \frac{d\Phi_{sq}}{dt} + (\omega_r - \omega) \cdot \psi_{sd}, \end{cases} \quad (8)$$

$$\begin{cases} \psi_{pd} = L_p \cdot I_{pd} + L_m \cdot I_{sd}; \\ \psi_{pq} = L_p \cdot I_{pq} - L_m \cdot I_{sq}; \\ \psi_{sd} = L_s \cdot I_{sd} + L_m \cdot I_{pd}; \\ \psi_{sq} = L_s \cdot I_{sq} - L_m \cdot I_{pq}. \end{cases} \quad (9)$$

The electromagnetic torque is expressed as:

$$T_e = \frac{3 \cdot P_r \cdot L_m}{2 \cdot L_p} \cdot (\psi_{pd} \cdot I_{sq} + \psi_{pq} \cdot I_{sd}). \quad (10)$$

The active and reactive powers equations at the primary stator, the secondary stator, and the grid are written as, respectively:

$$\begin{cases} P_p = \frac{3}{2} \cdot (U_{pd} \cdot I_{pd} + U_{pq} \cdot I_{pq}) \\ Q_p = \frac{3}{2} \cdot (U_{pq} \cdot I_{pd} - U_{pd} \cdot I_{pq}) \end{cases} \quad (11)$$

$$\begin{cases} P_s = \frac{3}{2} \cdot (U_{sd} \cdot I_{sd} + U_{sq} \cdot I_{sq}) \\ Q_s = \frac{3}{2} \cdot (U_{sq} \cdot I_{sd} - U_{sd} \cdot I_{sq}) \end{cases} \quad (12)$$

$$\begin{cases} P_g = P_p + P_s; \\ Q_g = Q_p + Q_s; \end{cases} \quad (13)$$

where U_p and U_s are power and control windings voltages in the dq axis, respectively; I_p and I_s are power and control windings currents in the dq axis, respectively; R_p and R_s are power and control windings resistances, respectively; L_p and L_s are leakage inductances of power and control windings, respectively; L_m is the mutual inductance between power and control windings; ω_p and ω_s are angular frequencies of the power and control windings, respectively; ω_r is the BDFRG mechanical rotor angular speed; ψ_p and ψ_s are power and control windings flux linkages in the dq axis, respectively.

5. Vector control of the BDFRG. In order to decouple the stator active and reactive powers, the primary stator flux vector will be aligned with d-axis φ_{pd} ($\varphi_{pd} = \varphi_p$ and $\varphi_{pq} = 0$), and the stator voltages will be expressed by:

$$\begin{cases} U_{pd} = 0; \\ U_{pq} = U_p = \omega_p \cdot \psi_p. \end{cases} \quad (14)$$

The expressions of the primary stator currents are written as:

$$\begin{cases} I_{pd} = \frac{\psi_{pd} - L_m \cdot I_{sd}}{L_p}; \\ I_{pq} = \frac{L_m \cdot I_{sq}}{L_p}. \end{cases} \quad (15)$$

By replacing these currents in the secondary stator fluxes equations, we obtain:

$$\begin{cases} \psi_{sd} = \sigma \cdot L_s \cdot I_{sd} + \frac{L_m}{L_p} \cdot \psi_{pd}; \\ \psi_{sq} = \sigma \cdot L_s \cdot I_{sq}. \end{cases} \quad (16)$$

where σ is the leakage coefficient defined by:

$$\sigma = 1 - \frac{L_m^2}{L_p \cdot L_s} \quad (17)$$

The secondary stator voltages can be written according to the secondary stator currents as:

$$\begin{cases} U_{sd} = R_s \cdot I_{sd} + L_s \cdot \sigma \cdot \frac{dI_{sd}}{dt} + e_d; \\ U_{sq} = R_s \cdot I_{sq} + L_s \cdot \sigma \cdot \frac{dI_{sq}}{dt} + e_d + e_\varphi, \end{cases} \quad (18)$$

where

$$\begin{cases} e_q = -\omega_s \cdot \sigma \cdot L_s \cdot I_{sq}; \\ e_d = \omega_s \cdot \sigma \cdot L_s \cdot I_{sd}; \\ e_\varphi = \omega_s \cdot \frac{L_m}{L_p} \cdot \psi_p. \end{cases} \quad (19)$$

The active and reactive stator powers of the BDFRG are expressed by:

$$\begin{cases} P_p = \frac{3}{2} \cdot \frac{U_{pq} \cdot L_m}{L_p} \cdot I_{sq}; \\ Q_p = \frac{3}{2} \cdot \frac{U_{pq}^2}{\omega_p \cdot L_p} - \frac{3}{2} \cdot U_{pq} \cdot \frac{L_m}{L_p} \cdot I_{sd}, \end{cases} \quad (20)$$

where s is the slip of the BDFRG.

The electromagnetic torque can be written as:

$$T_e = \frac{3 \cdot P_r \cdot L_m}{2 \cdot L_p} \cdot \psi_{pd} \cdot I_{sq}. \quad (21)$$

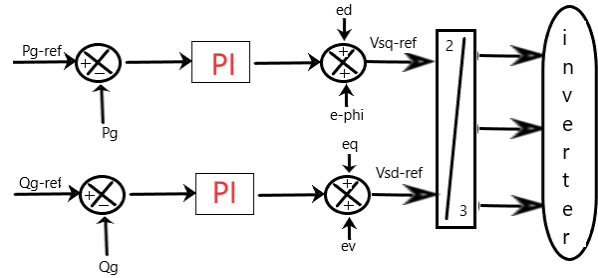


Fig. 4. Block diagram of power control

For relatively weak sleep values and by neglecting the voltage drops, the grid active and reactive powers are simplified into:

$$\begin{cases} P_g = \frac{3 \cdot (1-s) \cdot U_{pq} \cdot L_m}{2 \cdot L_p} \cdot I_{sq}; \\ Q_g = \frac{3}{2} \cdot \frac{U_{pq}^2}{\omega_p \cdot L_p} - \frac{3 \cdot (1-s)}{2} \cdot U_{pq} \cdot \frac{L_m}{L_p} \cdot I_{sd}. \end{cases} \quad (22)$$

From (22) we have:

$$\begin{cases} I_{sq} = \frac{2 \cdot L_p}{3 \cdot (1-s) \cdot U_{pq} \cdot L_m} \cdot P_g; \\ I_{sd} = \frac{\left(\frac{3 \cdot U_{pq}^2}{2 \cdot \omega_p \cdot L_p} - Q_g \right) \cdot 2 \cdot L_p}{3 \cdot (1-s) \cdot U_{pq} \cdot L_m}. \end{cases} \quad (23)$$

Substitute (23) in (18), we obtain:

$$\begin{cases} \dot{P}_g = \frac{U_{sq}}{A \cdot L_s \cdot \sigma} - \frac{R_s}{L_s \cdot \sigma} \cdot P_g - \frac{e_d}{A \cdot L_s \cdot \sigma} - \frac{e_\varphi}{A \cdot L_s \cdot \sigma}; \\ \dot{Q}_g = \frac{-U_{sd}}{A \cdot L_s \cdot \sigma} - \frac{R_s}{L_s \cdot \sigma} \cdot Q_g + \frac{e_q}{A \cdot L_s \cdot \sigma} + \frac{e_v}{A \cdot L_s \cdot \sigma}, \end{cases} \quad (24)$$

where

$$\begin{cases} A = \frac{2 \cdot L_p}{3 \cdot (1-s) \cdot U_{pq} \cdot L_m}; \\ e_v = A \cdot R_s \cdot \frac{3 \cdot U_{pq}^2}{2 \cdot \omega_p \cdot L_p}. \end{cases} \quad (25)$$

In order to capture the optimal mechanical power, the control of the mechanical speed is applied (Fig. 5).

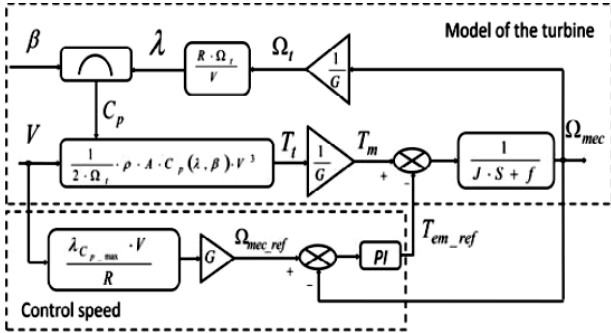


Fig. 5. MPPT with the control of the speed

The reference value of the active power exchanged between the wind generator and the grid is generated by MPPT control, and it's given by:

$$P_{g-ref} = T_{em-ref} \cdot \Omega_{mech}. \quad (26)$$

The reference grid reactive power Q_{g-ref} is fixed to zero value to maintain the power factor at unity. The detailed scheme of the studied system is illustrated in Fig. 6.

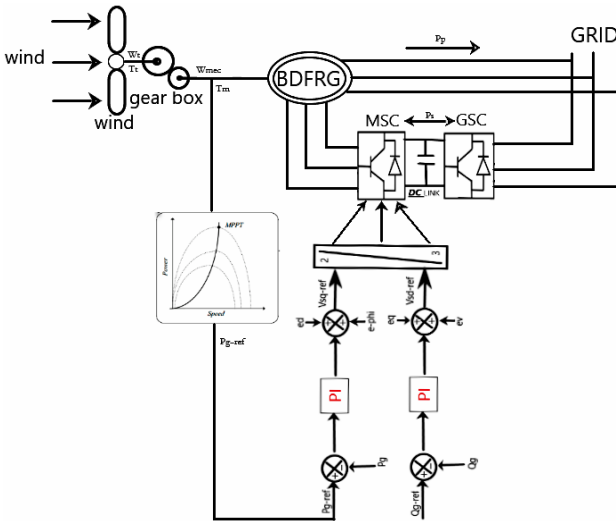


Fig. 6. The scheme of BDFRG using vector control

6. Sliding mode control. A Sliding Mode Controller (SMC) is a Variable Structure Controller (VSC) [28], which VSC includes several different continuous functions that can map plant state to a control surface, whereas switching among different functions is determined by plant state represented by a switching function [29]. The design of the control system will be demonstrated for the following nonlinear system:

$$\dot{X} = f(x,t) + B(x,t) \cdot u(x,t), \quad (27)$$

where $X \in R^n$ is the state vector; $u \in R^m$ is the control vector; $f(x,t) \in R^n$; $B(x,t) \in R^{n \times m}$.

From the system (16), it possible to define a set S of the state trajectories X such as:

$$S = \{x(t) | \sigma(x,t) = 0\}, \quad (28)$$

where

$$\sigma(x,t) = [\sigma_1(x,t), \sigma_2(x,t), \dots, \sigma_m(x,t)]^T, \quad (29)$$

where T denotes the transposed vector; S is called the sliding surface.

To bring the state variable to the sliding surfaces, the following two conditions have to be satisfied:

$$\sigma(x,t) = 0; \quad \dot{\sigma}(x,t) = 0. \quad (30)$$

The control law satisfies the precedent conditions is presented in the following form:

$$\begin{cases} U = U_{eq} + U_n; \\ U_n = -K_f \cdot \text{sgn}(\sigma(x,t)), \end{cases} \quad (31)$$

where U is the control vector; U_{eq} is the equivalent control vector; U_n is the switching part of the control (the correction factor); K_f is the controller gain.

U_{eq} can be obtained by considering the condition for the sliding regimen, $\sigma(x,t) = 0$. The equivalent control keeps the state variable on the sliding surface, once they reach it. For a defined function φ :

$$\text{sgn}(\varphi) = \begin{cases} 1, & \text{if } \varphi > 0; \\ 0, & \text{if } \varphi = 0; \\ -1, & \text{if } \varphi < 0. \end{cases} \quad (32)$$

The controller described by (29) presents high robustness, insensitive to parameter fluctuations and disturbances. However, it will have high-frequency switching (chattering phenomena) near the sliding surface due to the (sgn) function involved. These drastic input changes can be avoided by introducing a boundary layer with width ξ . Thus replacing $\text{sgn}(\sigma(t))$ by saturation function $\text{sat}(\sigma(t)/\xi)$ in (29) we have

$$U = U_{eq} - K_f \cdot \text{sat}(\sigma(x,t)), \quad (33)$$

where $\xi > 0$

$$\text{sat}(\varphi) = \begin{cases} \text{sgn}(\varphi), & \text{if } |\varphi| \geq 1; \\ \varphi, & \text{if } |\varphi| < 1. \end{cases} \quad (34)$$

Consider a Lyapunov function:

$$V = \frac{1}{2} \cdot \sigma^2. \quad (35)$$

From the Lyapunov theorem we know that if \dot{V} is negative definite, the system trajectory will be driven and attracted toward the sliding surface and remain sliding on it until the origin is reached asymptotically:

$$\dot{V} = \frac{1}{2} \cdot \frac{d\sigma}{dt} = \dot{\sigma} \cdot \sigma \leq -\eta \cdot |\sigma|, \quad (36)$$

where η is the constant positive value.

In this work we use the sliding surface proposed by J.J. Slotine

$$\sigma(x,t) = \left(\frac{d}{dt} + \gamma \right)^{n-1} \cdot e, \quad (37)$$

where

$x = [x, \dot{x}, \ddot{x}, \dots, x^{(n-1)}]$ is the state vector;

$x^d = [x^d, \dot{x}^d, \ddot{x}^d, \dots, x^{d(n-1)}]$ is the desired state vector;

$e = x^d - x = [e, \dot{e}, \ddot{e}, \dots, e^{(n-1)}]$ is the error vector;

γ is a positive coefficient; n is the system order [28].

In BDFRG control using sliding mode theory the surface is chosen as a function of the error between the reference input signal and the measured signals.

7. Sliding mode control of the BDFRG. The mathematical model of the grid active and reactive powers in (24) has two vector controls, so we define two switching surfaces, and we set $n = 1$. According to (37) the switching surfaces of the stator powers are given by:

$$\begin{cases} S(P_g) = e(P_g) = P_{g-ref} - P_g; \\ S(Q_g) = e(Q_g) = Q_{g-ref} - Q_g. \end{cases} \quad (38)$$

The second step consists of giving the structure of the vector control. One of the possible solutions is given by:

$$U_c = U_{eq} + U_n; \quad (39)$$

$$\begin{cases} U_{sq} = U_{sreq} + U_{sqn}; \\ U_{sd} = U_{sdeq} + U_{sdn}. \end{cases} \quad (40)$$

where U_{eq} (U_{sreq} , U_{sdeq}) and U_n (U_{sqn} , U_{sdn}) indicate the equivalent and discontinuous components of the control input vector U_c (U_{sq} and U_{sd}), respectively.

U_{eq} is calculated from $\dot{S}(x) = 0$

$$\dot{S}(x) = 0 \Rightarrow \begin{cases} \dot{S}(P_g) = \dot{P}_{g-ref} - \dot{P}_g = 0; \\ \dot{S}(Q_g) = \dot{Q}_{g-ref} - \dot{Q}_g = 0. \end{cases} \quad (41)$$

Substituting (24) in (41) we will have:

$$\begin{cases} \dot{P}_{g-ref} - \left(\frac{U_{sq}}{A \cdot L_s \cdot \sigma} - \frac{R_s}{L_s \cdot \sigma} \cdot P_g - \frac{e_d}{A \cdot L_s \cdot \sigma} - \frac{e_\phi}{A \cdot L_s \cdot \sigma} \right) = 0; \\ \dot{Q}_{g-ref} - \left(\frac{-U_{sd}}{A \cdot L_s \cdot \sigma} - \frac{R_s}{L_s \cdot \sigma} \cdot Q_g + \frac{e_q}{A \cdot L_s \cdot \sigma} + \frac{e_v}{A \cdot L_s \cdot \sigma} \right) = 0. \end{cases} \quad (42)$$

Replaced U_{sq} and U_{sd} from (40) in (42) we obtain:

$$\begin{cases} \dot{P}_{g-ref} - \left(\frac{U_{sreq} + U_{sqn}}{A \cdot L_s \cdot \sigma} - \frac{R_s}{L_s \cdot \sigma} \cdot P_g - \frac{e_d}{A \cdot L_s \cdot \sigma} - \frac{e_\phi}{A \cdot L_s \cdot \sigma} \right) = 0; \\ \dot{Q}_{g-ref} - \left(\frac{-U_{sdeq} + U_{sdn}}{A \cdot L_s \cdot \sigma} - \frac{R_s}{L_s \cdot \sigma} \cdot Q_g + \frac{e_q}{A \cdot L_s \cdot \sigma} + \frac{e_v}{A \cdot L_s \cdot \sigma} \right) = 0. \end{cases} \quad (43)$$

In the permanent regime $U_n = 0$ ($U_{sqn} = 0$ and $U_{sdn} = 0$). Replaced them in (43) and we extract U_{sreq} and U_{sdeq} :

$$\begin{cases} U_{sreq} = A \cdot L_s \cdot \sigma \cdot \dot{P}_{g-ref} + A \cdot R_s \cdot P_g - (e_d - e_\phi); \\ U_{sdeq} = -A \cdot L_s \cdot \sigma \cdot \dot{Q}_{g-ref} - A \cdot R_s \cdot Q_g + (e_q + e_v). \end{cases} \quad (44)$$

U_{sqn} and U_{sdn} are achieved by the condition:

$$S(x) \cdot \dot{S}(x) < 0 \Rightarrow S(P_g) \cdot \dot{S}(P_g) < 0 \text{ and } S(Q_g) \cdot \dot{S}(Q_g) < 0 \quad (45)$$

$$\begin{cases} \frac{-1}{A \cdot \sigma \cdot L_s} \cdot U_{sqn} \cdot S(P_g) < 0; \\ \frac{1}{A \cdot \sigma \cdot L_s} \cdot U_{sdn} \cdot S(Q_g) < 0. \end{cases} \quad (46)$$

A simple used form of U_n is a relay function:

$$U_n = -k \cdot \text{sgn}(S(x)); \quad (47)$$

$$\begin{cases} U_{sqn} = -k_1 \cdot \text{sgn}(S(P_g)); \\ U_{sdn} = -k_2 \cdot \text{sgn}(S(Q_g)). \end{cases} \quad (48)$$

where k (k_1 , k_2) must be positive to satisfy the previous condition.

Substituting (44) and (48) into (40) we obtain the expressions of the reference rotor voltages such as:

$$\begin{cases} U_{rq} = A \cdot L_s \cdot \sigma \cdot \dot{P}_{g-ref} + A \cdot R_s \cdot P_g - (e_d - e_\phi) - k_1 \cdot \text{sgn}(S(P_g)); \\ U_{rd} = -A \cdot L_s \cdot \sigma \cdot \dot{Q}_{g-ref} - A \cdot R_s \cdot Q_g + (e_q + e_v) - k_2 \cdot \text{sgn}(S(Q_g)). \end{cases} \quad (49)$$

The reference value of the active power exchanged between the wind generator and the grid is generated by MPPT control and it has given by (26). The reference grid reactive power Q_{g-ref} is fixed to zero value to maintain the power factor at unity. The detailed scheme of the studied system is illustrated in Fig. 7.

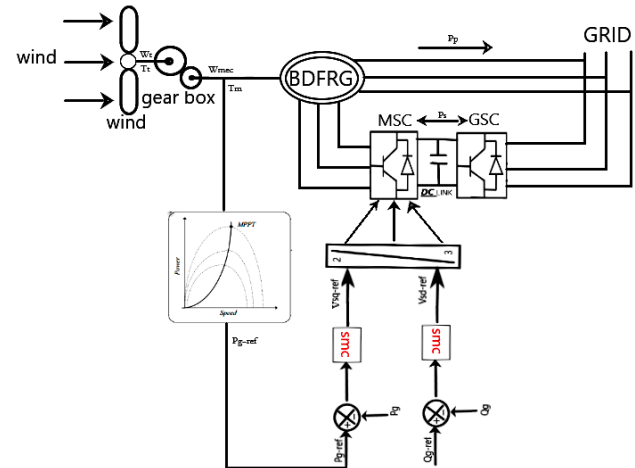


Fig. 7. The scheme of BDFRG using the sliding mode controller

8. Results and interpretations. The control technique suggested in this paper has been approved by the Matlab/Simulink software. The generator used in this simulation is 4.5 kW. This generator is connected directly to the grid through its primary stator and controlled through its secondary stator. Rated parameters are next [5]: $R_p = 3.781 \Omega$, $R_s = 2.441 \Omega$, $L_p = 0.41 \text{ H}$, $L_s = 0.316 \text{ H}$, $L_m = 0.3 \text{ H}$, $J = 0.2 \text{ kg} \cdot \text{m}^2$, $P_r = 4$. Wind turbine parameters are next: blade radius $R = 4 \text{ m}$, gearbox ratio $G = 7.5$, turbine inertia $1.5 \text{ kg} \cdot \text{m}^2$, air density $\rho = 1.225 \text{ kg/m}^3$ and number of blades is 3.

Figure 8 indicates the speed of the wind. The mechanical speed generated by the turbine is similar to the wind profile applied to the turbine. The reference value P_{g-ref} of the grid active power is determined by (26), and the reference of the reactive power is maintained at zero to guarantee unity power factor.

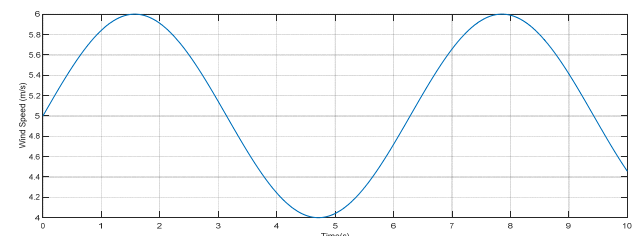


Fig. 8. Wind speed

Figures 9 demonstrate the performances of the vector control and SMC of the grid active and reactive powers used to a wind turbine mechanism structured from a BDFRG.

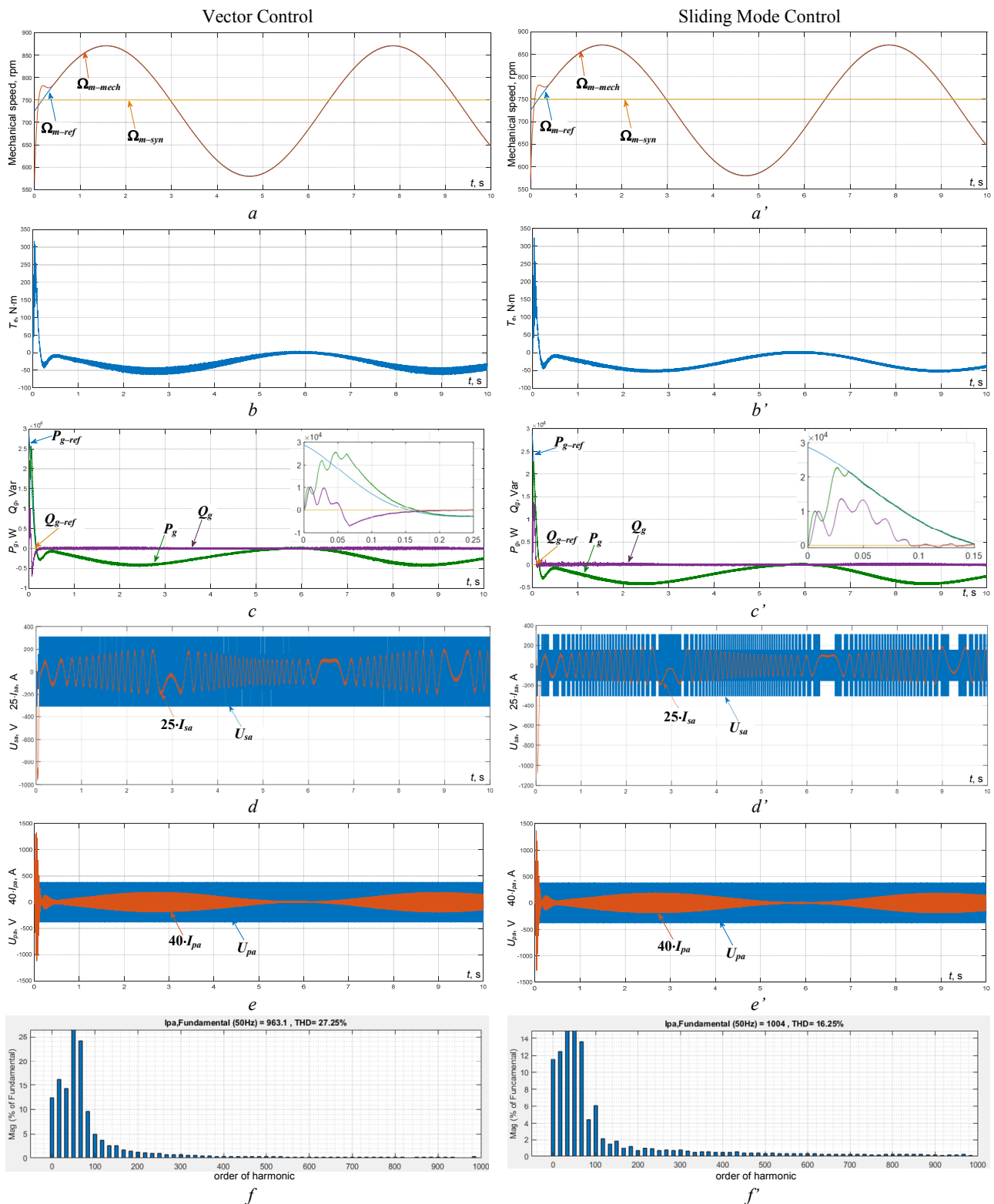


Fig. 9. Vector control and sliding mode control of the BDFRG:
a and *a'* – mechanical speed; *b* and *b'* – electromagnetic torque; *c* and *c'* – grid active and reactive power; *d* and *d'* – secondary stator phase voltage and current; *e* and *e'* – primary stator phase voltage and current; *f* and *f'* – total harmonic distortion of line current

Both control strategies approve an idealist decoupling between both elements of the BDFRG power (active and reactive). The outcomes found, without any doubt, demonstrate that the usage of the two commands can maintain the active and reactive powers to their aimed values. Figure 9 is the simulation results for active and reactive power response in using MPPT when the

traditional PI controller (Fig. 9,*a–e*) and sliding mode control (Fig. 9,*a'–e'*) are applied. In this study, simulation results show clearly the improvement of active and reactive power demand obtained by applying sliding mode control in terms of time response and good reference tracking accuracy than those obtained using the traditional PI regulator. In the case of star-up, we notice

that the sliding mode controller transient responses of both active and reactive powers present no overshoot, whereas the steady-state error is close to zero.

Figures 9,d,e and Fig. 9,d',e' present the winding currents in which we observe that both the frequency and the amplitude of these control currents (secondary currents I_s) change during the period of variation of active and reactive powers. On the other hand, the frequency of

the current of the supply winding (primary currents I_p) remains constant to be adapted to the supply frequency of the grid, so when the reference of the active power is changed, the amplitude of the current also is changed.

Robustness tests. Figure 10 represents a comparison between the two controllers robustness: PI and SMC with parametric variations L_p , L_s , R_s and L_m of -20% and $+20\%$ of their nominal values.

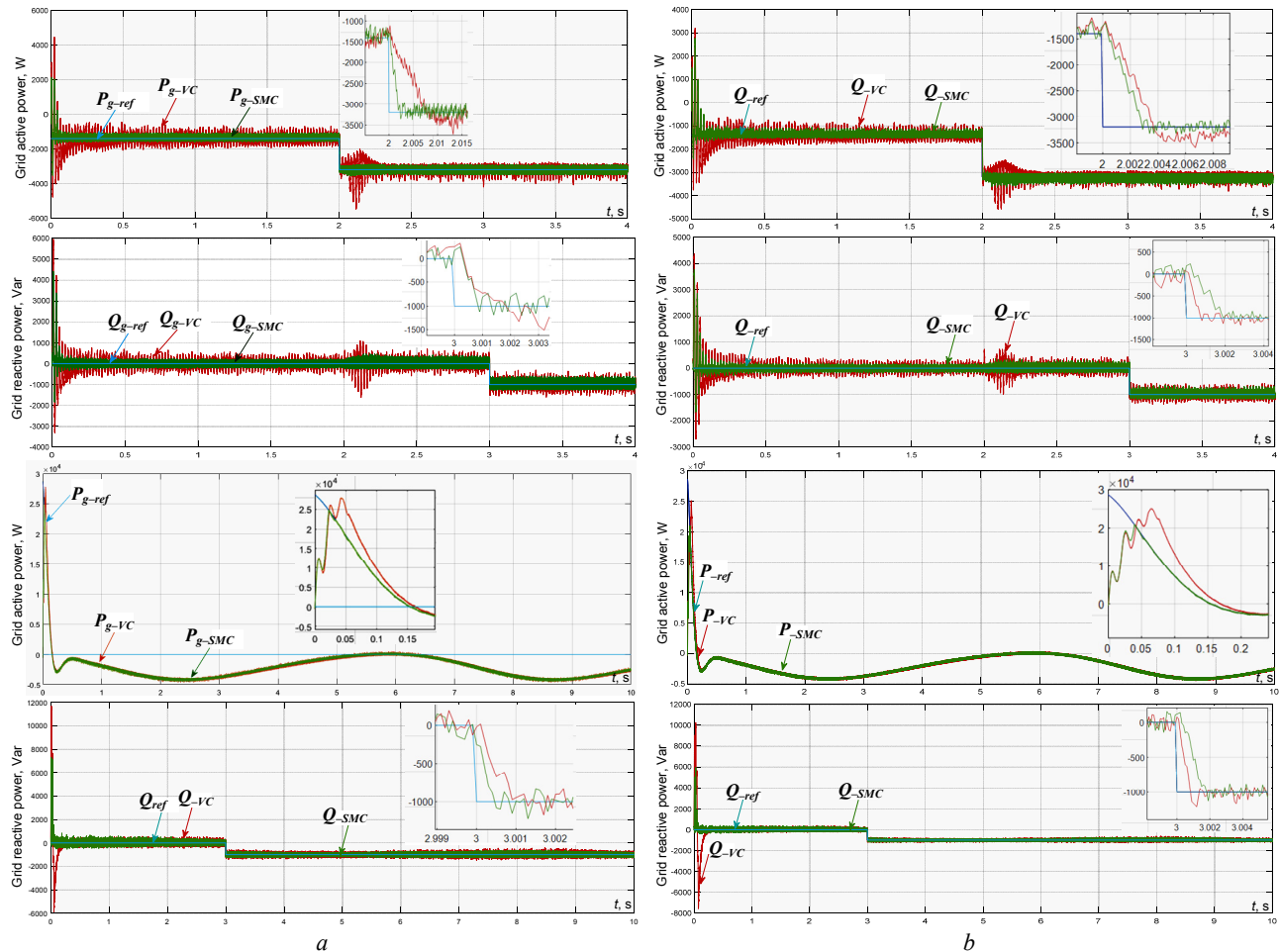


Fig. 10. Comparison of robustness between power control with PI and SMC of BDFRG with parametric variations L_p , L_s , R_s and L_m of -20% (a) and $+20\%$ (b) of their nominal values

From the obtained results (Fig. 10,a and Fig. 10,b) the SMC strategy is better than the vector control with PI in terms of response time and reference tracking.

Conclusions. This paper has presented a comparative study between two controllers of active and reactive powers for the wind energy system equipped with a brushless doubly fed reluctance generator. The first one is a proportional-integral controller, and the second is a sliding mode controller-based field oriented control strategy.

Simulation results show the optimized performances of the vector control strategy based on a sliding mode controller. We observe high performances in terms of response time for vector control is 0.2 s and for sliding mode is 0.04 s. Spectral analysis of line current shows that total harmonic distortion of vector control is 27.25 % unlike sliding mode able to reduce the total harmonic distortion to a low value of around 16.25 % (without filter) and reference tracking without overshoots through the response characteristics. The decoupling, the stability, and the convergence towards the equilibrium are assured. Furthermore, this regulation presents a high dynamic

response, and it is more robust against parameter variation of the brushless doubly fed reluctance generator versus the conventional proportional-integral controller.

Conflict of interest. The authors declare that they have no conflicts of interest.

REFERENCES

1. Hasan M.S. *Control of Brushless Doubly-Fed Reluctance Machines under Normal and Faulty Operating Conditions*. Doctoral thesis. University of Northumbria at Newcastle, United Kingdom, 2014. Available at: <https://nrl.northumbria.ac.uk/id/eprint/21433/> (Accessed 23.06.2021).
2. Boumassata A., Kerdoun D. Direct powers control of DFIG through direct converter and sliding mode control for WECS. *2015 3rd International Conference on Control, Engineering & Information Technology (CEIT)*, 2015, pp. 1-5. doi: <https://doi.org/10.1109/CEIT.2015.7233058>.
3. Tapia A., Tapia G., Ostolaza J.X., Saenz J.R. Modeling and control of a wind turbine driven doubly fed induction generator. *IEEE Transactions on Energy Conversion*, 2003, vol. 18, no. 2, pp. 194-204. doi: <https://doi.org/10.1109/TEC.2003.811727>.

4. Wu B., Lang Y., Zargari N., Kouro S. *Power Conversion and Control of Wind Energy Systems*. The Institute of Electrical and Electronics Engineers, 2011. doi: <https://doi.org/10.1002/9781118029008>.
5. Mousa M.G., Allam S.M., Rashad E.M. Vector control strategy for maximum wind-power extraction of a grid-connected wind-driven Brushless Doubly-Fed Reluctance Generator. *2015 4th International Conference on Electric Power and Energy Conversion Systems (EPECS)*, 2015, pp. 1-6. doi: <https://doi.org/10.1109/EPECS.2015.7368515>.
6. Tazil M., Kumar V., Bansal R.C., Kong S., Dong Z.Y., Freitas W. Three-phase doubly fed induction generators: an overview. *IET Electric Power Applications*, 2010, vol. 4, no. 2, p. 75. doi: <https://doi.org/10.1049/iet-epa.2009.0071>.
7. Kim H.S., Lu D.D.-C. Review on wind turbine generators and power electronic converters with the grid-connection issues. *AUPEC 2010 – 20th Australasian Universities Power Engineering Conference: «Power Quality for the 21st Century»*, 2010, art. no. 5710761. Available at: <https://ieeexplore.ieee.org/document/5710761/> (Accessed 23.06.2021).
8. Iov F., Ciobotaru M., Blaabjerg F. Power electronics control of wind energy in distributed power systems. *2008 11th International Conference on Optimization of Electrical and Electronic Equipment*, 2008, pp. XXIX-XLIV. doi: <https://doi.org/10.1109/OPTIM.2008.4602332>.
9. Arifi E. *Modelling & Simulation of a Wind Turbine with Doubly-Fed Induction Generator (DFIG)*. Thesis, November 2020.
10. Cheng M., Han P., Buja G., Jovanović M.G. Emerging Multiport Electrical Machines and Systems: Past Developments, Current Challenges, and Future Prospects. *IEEE Transactions on Industrial Electronics*, 2018, vol. 65, no. 7, pp. 5422-5435. doi: <https://doi.org/10.1109/TIE.2017.2777388>.
11. Jovanović M., Ademi S., Llano D.X. Control of Doubly-Fed Reluctance Machines without a Shaft Position or Speed Sensor. *2018 International Symposium on Power Electronics, Electrical Drives, Automation and Motion (SPEEDAM)*, 2018, pp. 1245-1250. doi: <https://doi.org/10.1109/SPEEDAM.2018.8445405>.
12. Agha Kashkooli M.R., Jovanović M.G. A MRAS Observer for Sensorless Operation of Grid-Connected BDFRG Wind Turbines. *2020 IEEE 29th International Symposium on Industrial Electronics (ISIE)*, 2020, pp. 1517-1522. doi: <https://doi.org/10.1109/ISIE45063.2020.9152461>.
13. Abdel-Khalik A., Elserougi A., Massoud A., Ahmed S. A power control strategy for flywheel doubly-fed induction machine storage system using artificial neural network. *Electric Power Systems Research*, 2013, vol. 96, pp. 267-276. doi: <https://doi.org/10.1016/j.epsr.2012.11.012>.
14. Bhutto D.K., Ahmed Ansari J., Hussain Bukhari S.S., Akhtar Chachar F. Wind energy conversion systems (WECS) generators: A review. *2019 2nd International Conference on Computing, Mathematics and Engineering Technologies (iCoMET)*, 2019, pp. 1-6. doi: <https://doi.org/10.1109/ICOMET.2019.8673429>.
15. Betz R.E., Jovanovic M. *Introduction to Brushless Doubly Fed Reluctance Machines – The Basic Equations*. Technical Report EE0023. 19 March 1998. doi: <http://dx.doi.org/10.13140/RG.2.1.2646.4483>.
16. Ademi S., Jovanović M.G., Hasan M. Control of Brushless Doubly-Fed Reluctance Generators for Wind Energy Conversion Systems. *IEEE Transactions on Energy Conversion*, 2015, vol. 30, no. 2, pp. 596-604. doi: <https://doi.org/10.1109/TEC.2014.2385472>.
17. Zhang A., Wang X., Jia W., Ma Y. Indirect Stator-Quantities Control for the Brushless Doubly Fed Induction Machine. *IEEE Transactions on Power Electronics*, 2014, vol. 29, no. 3, pp. 1392-1401. doi: <https://doi.org/10.1109/TPEL.2013.2260870>.
18. Cardenas R., Pena R., Alepuz S., Asher G. Overview of Control Systems for the Operation of DFIGs in Wind Energy Applications. *IEEE Transactions on Industrial Electronics*, 2013, vol. 60, no. 7, pp. 2776-2798. doi: <https://doi.org/10.1109/TIE.2013.2243372>.
19. Jovanovic M. Sensorless and sensorless speed control methods for brushless doubly fed reluctance motors. *IET Electric Power Applications*, 2009, vol. 3, no. 6, p. 503-513. doi: <https://doi.org/10.1049/iet-epa.2008.0227>.
20. Jovanovic M.G., Jian Yu, Levi E. Encoderless direct torque controller for limited speed range applications of brushless doubly fed reluctance motors. *IEEE Transactions on Industry Applications*, 2006, vol. 42, no. 3, pp. 712-722. doi: <https://doi.org/10.1109/TIA.2006.872955>.
21. Chaal H., Jovanovic M. Toward a Generic Torque and Reactive Power Controller for Doubly Fed Machines. *IEEE Transactions on Power Electronics*, 2012, vol. 27, no. 1, pp. 113-121. doi: <https://doi.org/10.1109/TPEL.2011.2160731>.
22. Chaal H., Jovanovic M. Practical Implementation of Sensorless Torque and Reactive Power Control of Doubly Fed Machines. *IEEE Transactions on Industrial Electronics*, 2012, vol. 59, no. 6, pp. 2645-2653. doi: <https://doi.org/10.1109/TIE.2011.2161065>.
23. Chaal H., Jovanovic M. Power control of brushless doubly-fed reluctance drive and generator systems. *Renewable Energy*, 2012, vol. 37, no. 1, pp. 419-425. doi: <https://doi.org/10.1016/j.renene.2011.06.011>.
24. Valenciaga F. Second order sliding power control for a variable speed-constant frequency energy conversion system. *Energy Conversion and Management*, 2010, vol. 51, no. 12, pp. 3000-3008. doi: <https://doi.org/10.1016/j.enconman.2010.06.047>.
25. Farid B., Tarek B., Sebti B. Fuzzy super twisting algorithm dual direct torque control of doubly fed induction machine. *International Journal of Electrical and Computer Engineering (IJECE)*, 2021, vol. 11, no. 5, p. 3782-3790. doi: <https://doi.org/10.11591/ijece.v11i5.pp3782-3790>.
26. Bekakra Y., Ben Attous D. A sliding mode speed and flux control of a doubly fed induction machine. *2009 International Conference on Electrical and Electronics Engineering - ELECO 2009*, 2009, pp. 1-174-1-178. doi: <https://doi.org/10.1109/ELECO.2009.5355328>.
27. Abid M., Aissaoui A.G., Bounoua H. Sliding mode application in speed and flux control of an induction machine. *Istanbul University - Journal of Electrical and Electronics Engineering*, 2006, vol. 6, no. 2, pp. 197-204.
28. Abderazak S., Farid N. Comparative study between Sliding mode controller and Fuzzy Sliding mode controller in a speed control for doubly fed induction motor. *2016 4th International Conference on Control Engineering & Information Technology (CEIT)*, 2016, pp. 1-6. doi: <https://doi.org/10.1109/CEIT.2016.7929044>.
29. Routray S.K., Nayak N., Rout P.K. A Robust Fuzzy Sliding Mode Control Design for Current Source Inverter based STATCOM Application. *Procedia Technology*, 2012, vol. 4, pp. 342-349. doi: <https://doi.org/10.1016/j.protcy.2012.05.052>.

Received 25.10.2021

Accepted 30.11.2021

Published 23.02.2022

Oualah Oussama¹, PhD Student,
Djallel Kerdoun¹, Professor,
Abderraouf Boumassata², Dr.,

¹ Electrical Engineering Laboratory of Constantine (LGEC),
Department of Electrical Engineering,
Mentouri Brothers University, Constantine 1,
Campus Ahmed Hamani Zerzara,
Constantine, 25000, Algeria
e-mail: oussama.oulha@umc.edu.dz (Corresponding author);
Kerdjallel@yahoo.fr

² Department of Electronics, Electrical Engineering and
Automation,
Laboratory of Electrical Engineering of Polytechnic School of
Constantine (LGEPCE),
National Polytechnic School of Constantine, Algeria
e-mail: a_boumassata@umc.edu.dz

How to cite this article:

Oualah O., Kerdoun D., Boumassata A. Comparative study between sliding mode control and the vector control of a brushless doubly fed reluctance generator based on wind energy conversion systems. *Electrical Engineering & Electromechanics*, 2022, no. 1, pp. 51-58. doi: <https://doi.org/10.20998/2074-272X.2022.1.07>.